Simultaneous Optical Measurement of Soot Volume Fraction and Temperature in Premixed Flames

M. Y. CHOI,* A. HAMINS, G. W. MULHOLLAND, and T. KASHIWAGI
Building and Fire Research Laboratory, National Institute of Standards and Technology, Gaithersburg, MD 20899

The performance of a three-wavelength optical probe technique for measuring soot volume fraction and temperature was assessed by conducting experiments in the homogeneous environment of a premixed flame. Using a premixed ethylene/air flame, the temperatures and soot volume fractions (f_{va}, based on absorption measurements at 633 nm and f_{ve}, based on emission measurements at 900 nm and 1000 nm) were compared with previously reported results. Although the temperatures and mean soot volume fractions compared favorably, the discrepancy between f_{va} and f_{ve} prompted new measurements to evaluate the importance of source wavelength on the f_{va} measurements, scattering by soot particles, light absorption by "large" molecules and the use of different indices of refraction reported in the literature. The experiments on the degree of soot scattering and light absorption by "large" molecules indicated that these effects cannot reconcile the observed discrepancy in the soot volume fractions. The measured soot volume fractions were, however, sensitive to the absorption constant and therefore varied significantly when different sets of refractive indices were used. Furthermore, the agreement between f_{va} and f_{ve} was improved when extinction measurements were performed with longer wavelength light sources. Isokinetic soot sampling experiments were also performed to compare with the optically-measured soot volume fractions. This technique does not rely on the refractive indices of soot and therefore provides an independent measure of the soot volume fraction. The soot volume fractions measured using this technique compared favorably with the optically measured values (calculated using various indices of refraction).

NOMENCLATURE

c speed of light
D_f fractal dimension
d_p primary particle size
F_λ wavelength-dependent character of the detection system
F angular correction factor
f_{ve} soot volume fraction based on emission
f_{va} soot volume fraction based on absorption
h Planck's constant
I_λ spectral radiation intensity
k wavenumber
K_λ soot absorption constant
k_λ imaginary part of the soot index of refraction
k_b Boltzmann's constant
L probe separation distance in transmission measurements
L' probe separation distance in emission measurements
m soot index of refraction
m_s mass of collected soot
n_λ real part of the soot index of refraction
R_g radius of gyration
T temperature
t collection period

Greek Symbols

α polarizability
ϕ equivalence ratio
θ scattering angle
ρ_s density of soot
ρ_{sa} scattering/absorption ratio
σ scattering coefficient
λ wavelength of light source

INTRODUCTION

In large pool fires, radiative heat transfer governs the burning and flame spread rates and therefore is a key factor in assessing potential

* Present address: University of Illinois at Chicago, Department of Mechanical Engineering, 842 W. Taylor St. (M/C 251), Chicago, IL 60607-7022.

0010-2180/94/$7.00

fire hazards. The radiative heat feedback from the flame to the fuel surface is controlled by the temperature and soot distribution inside the fire. Early attempts at modeling this process involved several limiting assumptions including the use of average flame emissivity and constant flame temperatures [1] or mean temperatures and absorption/emission coefficients as a function of height and effective flame shapes [2]. Due to the turbulent nature of these fires, the use of mean radiative properties can lead to significant differences between the predicted and measured fuel burning rates [3]. Markstein [4] investigated spatial and temporal variations of the emission intensity for pool fires and discussed the importance of turbulent fluctuations of temperatures and soot volume fractions on radiation. Thus, direct integration of the turbulent radiative heat transfer equation requires the localized instantaneous temperature and emissivity distributions within the region between the fuel surface and the flame [5, 6].

In an attempt to characterize turbulence-radiation interactions, Klassen et al. [7] utilized a three-wavelength optical probing technique in a small pool fire burning toluene. This method employs a two-wavelength emission measurement for temperature and soot volume fraction [8], f_{ve}, and concurrent laser extinction for measurement of the soot volume fraction based on absorption, f_{va} [9]. It has been reported that the uncertainties in the measured values of T, f_{ve}, and f_{va} are functions of the magnitude of the measured values [9]. Thus, in a large pool fire, the resulting uncertainties in the measurements are likely to be different from the case in which small pool fires were studied by Klassen et al. [7]. Therefore, a rigorous assessment of the accuracy of this measurement technique was required for its eventual use in large pool fires burning toluene and heptane.

In this study, the performance of the three-wavelength technique was tested in a homogeneous path-invariant environment of premixed hydrocarbon/air flames. Under this condition, the soot volume fraction based on absorption, f_{va}, can be compared directly to the soot volume fraction based on emission, f_{ve}. In a non-homogeneous environment, f_{ve}, represents the Planck-weighted average (and therefore is biased toward the hotter soot particles) whereas f_{va} is the average soot volume fraction in the pathlength. Thus, in a non-homogeneous environment such as a fluctuating pool fire, f_{ve} will be different from f_{va}. However, in the path-invariant environment of a premixed flame, the two techniques should provide the same value of soot volume fraction.

THREE-WAVELENGTH TECHNIQUE

The soot volume fraction based on absorption, f_{va}, is determined from the measurement of the transmittance through the flame,

$$\frac{I_\lambda}{I_{\lambda 0}} = e^{-\frac{K_\lambda(1+\rho_{sa})f_{va}L}{\lambda}}, \tag{1}$$

where K_λ is the absorption constant, λ is the wavelength of the incident ($I_{\lambda 0}$) and transmitted (I_λ) radiation intensity, and L is the path length. Initially, the scattering to absorption ratio, ρ_{sa}, was assumed to equal zero. The absorption constants were calculated from the dispersion relationship of Dalzell and Sarofim [10] using the following equation:

$$K_\lambda = \frac{36\pi n_\lambda k_\lambda}{(n_\lambda^2 - k_\lambda^2 + 2)^2 + 4n_\lambda^2 k_\lambda^2} \tag{2}$$

where n_λ and k_λ are the wavelength-dependent real and imaginary parts of the complex index of refraction, respectively.

The emission intensity for the two wavelength regions used here are given by:

$$I_{900} = \frac{\int_{\lambda_l}^{\lambda_u} I_{b\lambda} F_{900\lambda}(1 - e^{-K_\lambda f_{ve} L'/\lambda})\, d\lambda}{\int_{\lambda_l}^{\lambda_u} F_{900\lambda}\, d\lambda}, \tag{3}$$

$$I_{1000} = \frac{\int_{\lambda_l}^{\lambda_u} I_{b\lambda} F_{1000\lambda}\left(1 - e^{-\frac{K_\lambda f_{ve} L'}{\lambda}}\right) d\lambda}{\int_{\lambda_l}^{\lambda_u} F_{1000\lambda}\, d\lambda}, \tag{4}$$

where λ_l and λ_u are the lower and upper cutoff wavelengths, respectively, for the interference filters, F_λ is the wavelength-dependent

characteristics of the detection system, L' is the pathlength, and $I_{b\lambda}$ is Planck's function:

$$I_{b\lambda} = \frac{2hc^2}{\lambda^5(e^{hc/\lambda k_b T} - 1)}, \quad (5)$$

where h is Planck's constant, c is the speed of light, k_b is Boltzmann's constant, and T is the temperature of the radiating particles. Equations 3 and 4 were solved for the two unknowns; temperature, T, and soot volume fraction, f_{ve}. Using a single set of refractive indices to calculate the absorption constant, the uncertainty in the temperature measurements is estimated to be approximately 50°C and the uncertainties in f_{ve} and f_{va} are approximately 10% which are similar to the values reported by Sivathanu et al. [9].

EXPERIMENTAL TECHNIQUE

Figure 1 displays the schematic diagram of the experimental apparatus. It is similar to that described by Klassen et al. [7] except that in the current system, light signals were carried through a trifurcated fiber optic bundle. This facilitates the movement of the probes through the fire. In the three-wavelength probe technique, the emission intensity from the luminous path length was monitored at wavelengths of 900 and 1000 nm (both with 60-nm half-bandwidths), while simultaneously measuring the transmission signal from a 633-nm He–Ne laser mechanically chopped at 400 Hz. The transmission signal was separated from the background emission by using a phase-loop lock-in amplifier. The emission signals were detected by two biased silicon photodiodes. The emission detection system was calibrated using a blackbody source operating at 1000°C. The calibration factors were checked frequently and were found to be constant before and after the experiments. The emission and transmission signals were acquired at 100 Hz for a period of 50 s.

The housings for the fiber optic bundle (probe A) and the absorption detector (probe B) were water-cooled (at 15°C). Portions of the light-guide tube that were inserted into the flame were not water-cooled to minimize the disturbance to the flame. To prevent deposition of soot particles, nitrogen was purged at approximately 0.8 cm^3/min through each light-guide. The light-guide was a coaxial assembly of a 135-mm-long stainless-steel tube (of 3.2 mm diameter) inserted into a larger stainless-steel tube (of 6.4 mm diameter) of the same length (denoted as Case A). This coaxial arrangement produced less background emission (caused by heating of the light-guides from the flame) in comparison to the case in which a single 6.4-mm tube was used (denoted as Case B). This was tested by subjecting it to a nonluminous Meeker Burner flame to cause the light-guide to radiate. The dotted line in Fig. 2 shows the emission intensity monitored at 1000

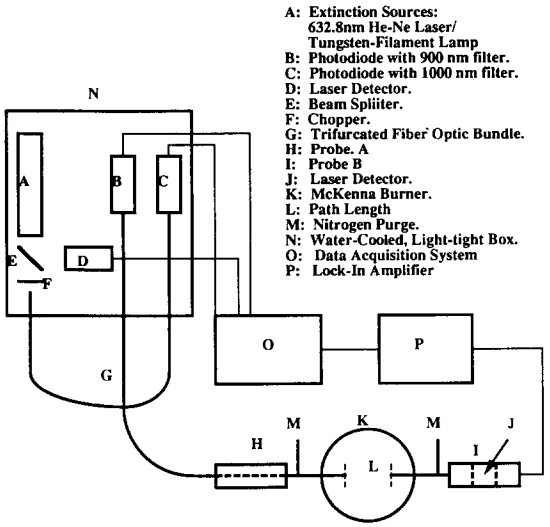

Fig. 1. Schematic of the three-wavelength experimental apparatus.

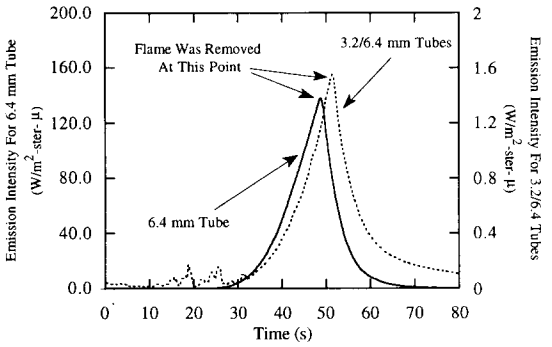

Fig. 2. Emission intensity at 1000 nm for cases using 6.4-mm tube and 3.2/6.4-mm tube combination as light-guides.

nm as a function of time after exposure to the flame for Case A. The solid line corresponds to the emission intensity measured for Case B. Within 30–40 s after the initiation of heating, the intensity from the glowing tube in Case B represented more than 25% of the emission signal from a typical luminous flame experiment. The measured radiation intensity measured for Case A was nearly two orders of magnitude lower than for Case B. In Case A, the inner tube shielded the detector from measuring the emission from the radiating outer tube, thereby greatly improving the signal to noise ratio of the measurements.

In this study and in the study by Klassen et al. [7], 1-mm dark zones were observed at the ends of the light-guides caused by quenching. These dark zones do not contribute to the overall emission measurements in the probe volume; however, the cool soot particles in this zone will still attenuate the laser signal and affect the absorption measurements. Thus, the path length L' used in Eqs. 3 and 4 is 2 mm less than the path length L used in Eq. 1.

PREMIXED FLAME EXPERIMENTS

The performance of the three-wavelength technique for measuring temperature and soot volume fraction was tested in a homogeneous environment of a premixed ethylene/air flame. In this experiment, the opposing probes were separated by 20 mm and were placed 25 mm above the burner surface. The fuel/air equivalence ratio was varied from 2.1 to 2.4. Figure 3 displays the measured soot volume fractions (f_{va} and f_{ve}) and temperatures as a function of equivalence ratio. The soot volume fraction based on emission and absorption increased as a function of equivalence ratio, however, f_{va} did not equal f_{ve}. The measured temperature, f_{va} and f_{ve} were compared to the results reported by Harris and Weiner [11] for the same experimental conditions (denoted by HW). Harris and Weiner measured the temperature using the Kurlbaum technique and the soot volume fraction using the scattering and extinction technique of D'Alessio and coworkers [12]. The mean soot volume fraction (mean of f_{ve} and f_{va}) compared favorably with the soot volume fractions reported by Harris and Weiner [11], with an average difference of less than 20% between the two sets of experiments. Furthermore, their reported temperature for $\phi = 2.3$ of 1610 K is also in good agreement with our experimental value of 1603 K.

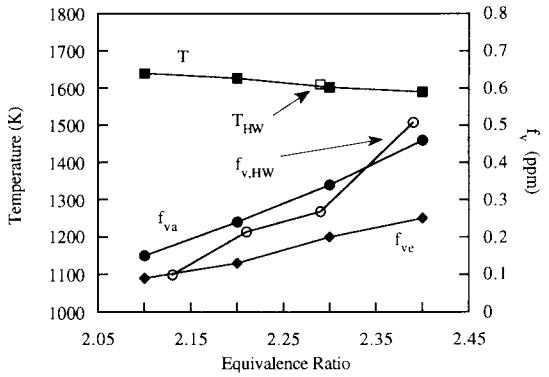

Fig. 3. Temperature, f_{va} and f_{ve}, based on K_λ from Ref. 10, compared with data reported Harris and Weiner (denoted as HW), Ref. 11.

Although the general agreement with the results of Harris and Weiner was encouraging, the difference between f_{va} and f_{ve} was cause for concern. It was thought that the difference in the soot volume fractions may have resulted from the possible nonuniform temperature distribution within the probe volume. For premixed flames, the path length of constant temperature and soot volume fraction decreases as a function of height above the burner [13]. To ensure a region of uniform temperature distribution, the probes were placed closer to the burner surface. To produce sufficient luminosity to perform the emission measurements and attenuation for the absorption measurements, a rich, premixed acetylene/air ($\phi = 2.3$) flame was investigated. The probe separation, L, was 20 mm and the probes were placed 8 mm above the burner surface. Figure 4 presents the measured temperature, f_{ve} and f_{va} as a function of radial position. Radial position of "0" corresponds to the center of the burner. The flat profiles of the temperature, f_{ve} and f_{va} in Fig. 4 indicate that uniform conditions existed within the path length. Thus, by definition, f_{va} should equal f_{ve} in this environment, however, f_{va} is greater than f_{ve} by nearly a factor of two. The most obvious factors causing the overprediction of f_{va} was thought to be

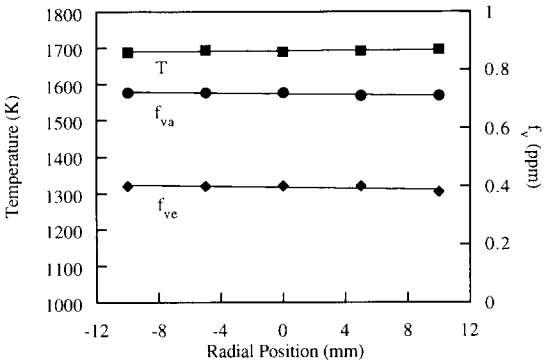

Fig. 4. Temperature, f_{va} and f_{ve} (using K_λ from Ref. 10) measured as a function of radial position. "0" corresponds to the center of the burner.

scattering by soot particles and light absorption by large polyaromatic hydrocarbon (PAH) molecules. The next sections describe experiments that were performed to assess the importance of these factors in reconciling the difference between f_{va} and f_{ve}.

ABSORPTION BY LARGE MOLECUELS

Large PAH molecules can absorb radiation in the visible and in the near-infrared range [14] and therefore cause overprediction of f_{va}. Weiner and Harris [15] defined several classes of PAHs that can coexist with the soot particulates: Class A, with molecular weights of ~ 1000 amu, are present in the soot inception zone; Class B, with molecular weights between ~ 500 and ~ 1000 amu, are present in the immediate postinception zone; and Class C, with molecular weights less than ~ 500 amu, are present in the postinception zone. Since the large Class A molecules are depleted at the soot particle inception zone, it is likely that most of the absorption by PAH molecules in the postinception region of a premixed flame (where optical measurements were made in the present study) are due to Class B or Class C molecules. The absorption spectra for these molecules could extend to 700 nm [14]; thus it is possible that the f_{va} measurements at 633 nm may have been affected by molecular absorption. However, it is believed that the contribution to the emission intensity by these molecules will be negligible compared with the emission intensity due to soot particles. To have an absorption/emission spectrum extending to 900 nm, the PAHs would have to be significantly larger than Class B molecules [11]. Thus, f_{ve} measured using emission from 900 and 1000 nm should not be affected by the presence of PAHs.

The importance of light absorption by PAHs was investigated by using radiation sources with wavelengths of 488 nm, 633 nm, 940 nm and 1550 nm. Figure 5 displays the measured f_{va} at these wavelengths for $\phi = 2.3$ acetylene/air flame at 8 mm above the burner surface. The experiment at 940 nm was performed using a series of infrared emitting diodes and a pair of narrow (10 nm half-bandwidth) filters to prevent interference with emission measurement at 900 and 1000 nm. The experiments at 488 and 1550 nm were performed using a tungsten filament lamp and pairs of interference filters.

The decrease of f_{va} at the longer source wavelengths was consistent with the presence of "large" absorbing molecules. Previous studies [15, 16] suggest that the fraction of absorption by PAH molecules (relative to absorption by soot) at wavelengths as high as 940 and 1550 nm should be negligible. Thus, the extinction of the light source due to PAH absorption can be estimated from the difference in the soot volume fraction measurements at 1550 nm and 488 nm. However, this was not deemed appropriate for our study due to possible scattering by soot particles (i.e., ρ_{sa} may not equal zero in Eq. 1) at the 488-nm wavelength. Thus, a method that is independent of scattering was

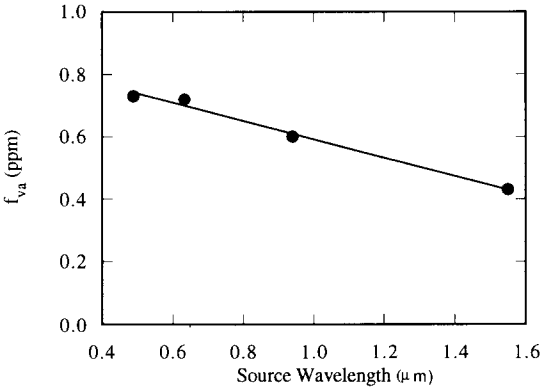

Fig. 5. f_{va} measurement (using K_λ from Ref. 10) at various source wavelengths.

needed to assess the importance of absorption by PAH molecules.

Using a rich atmospheric pressure premixed methane/oxygen flame, D'Alessio et al. [12] found that the ratio of the concentration of PAH to soot decreased as a function of height above the burner. Since, the f_{ve} based on measurements at 900 and 1000 nm should not be affected by the presence of Class B/Class C molecules, the ratio of f_{va}/f_{ve} is expected to decrease with height as the concentration of large molecules decreases. Figure 6 displays measurements of f_{va} (using 633 nm He–Ne laser) and f_{ve} as a function of height above the burner surface for a premixed acetylene/air flame ($\phi = 2.3$, $L = 20$ mm). If significant PAH absorption occurred in the measurements at positions close to the burner surface, the ratio of f_{va}/f_{ve} would have decreased as a function of height above the burner. The data in Fig. 6 indicate that both f_{va} and f_{ve} increased as a function of height and that the ratio of the soot volume fractions remained nearly constant to within the uncertainty in the measurements. Thus, this experiment suggests that absorption by PAH does not contribute significantly to the discrepancy in the soot volume fractions.

SOOT SCATTERING EXPERIMENTS

For the measurements shown in Figs. 3–5, the scattering component of extinction was discounted by assuming that the soot particles were much smaller than the wavelength of the incident light. However, the Rayleigh limit solution is valid for cases in which the optical size, $\pi d_p/\lambda$, is typically less than about 0.3. Analysis of transmission electron micrographs [TEM] of soot collected using thermophoretic probes at various positions above the burner surface indicates that the primary particle sizes encountered in our experiments were much smaller than the extinction source wavelength. The measured primary particle sizes were 18, 21, and 23 nm at positions 8, 15, and 25 mm above the burner surface, respectively, for $\phi = 2.3$. However, agglomeration of individual soot particles can result in large aggregates (consisting of hundreds of primary particles) with optical sizes much greater than unity. Under such conditions, scattering can account for a significant fraction of the signal attenuation and can lead to overprediction of f_{va}. For example, Köylü and Faeth [17] found that the scattering-to-absorption ratio can be as large as unity for soot in the overfire region of acetylene and toluene diffusion flames for a source wavelength of 633 nm.

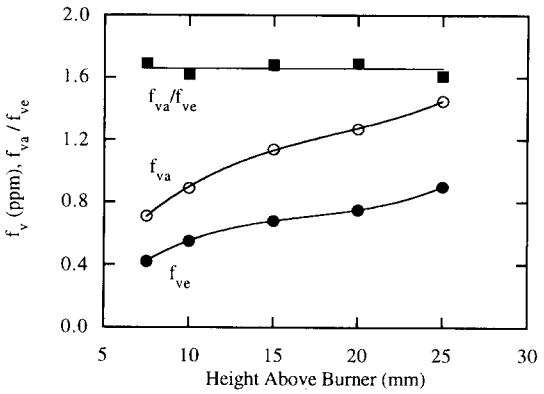

Fig. 6. f_{va}, f_{ve} and f_{va}/f_{ve} (using K_λ from Ref. 10) measured as a function of height above the burner.

In order to assess the degree of scattering in the current experiments, differential scattering measurements were performed. The polarization direction of the 5-W argon-ion laser was set at 45° to emulate natural light (corresponding to two linearly-polarized orthogonal beams). The detection optics included a 5-mm aperture, interference filter, 9-cm focal length lens, 1-mm pinhole, polarizer, diffuser, and a photomultiplier tube. The acceptance angle of the optics was approximately 0.6°. The detection optics assembly was attached to a motorized rotary table (controlled by the data acquisition system) that was positioned concentrically below the burner.

The total scattered intensity was measured as a function of scattering angle, θ, with $\theta = 0$ corresponding to forward scattering. Figure 7 displays the total scattered intensity measurements for the various conditions. Repeatability of the measurements is shown for the $\phi = 2.3$ experiment at a height of 8 mm. The scattered intensity was measured from 20° to 90° at 10° intervals. (For discussions of approximations used to determine the scattering intensity, see Appendix I). At every angular position, the

detection system was calibrated by measuring the scattered intensities of propane ($I'_{\text{prop},s}$), nitrogen ($I'_{N_2,s}$) and helium ($I'_{\text{He},s}$). The intensities measured for helium were attributed to laser reflections from the surroundings (due to its small scattering cross-section). Therefore, the scattered intensity for helium was subtracted from the intensities measured for propane and nitrogen. The theoretical scattering cross-section ratio of propane to nitrogen is 10.9 at 488 nm calculated with the indices of refraction given by Landolt-Börenstein [18]. The measured scattering cross-section ratio, calculated from the relationship

$$\frac{I_{\text{Prop},s}}{I_{N_2,s}} = \frac{(I'_{\text{Prop},s} - I'_{\text{He},s})}{(I'_{N_2,s} - I'_{\text{He},s})} \tag{6}$$

was 11.0 ± 0.31. For a Rayleigh scatterer such as propane, the angular variation of the scattered intensity follows the relationship

$$I_{\text{Prop},s}(\theta) = I_{\text{Prop},s}(90°)[1 + \cos^2\theta]. \tag{7}$$

At each angular position, the scattered intensity for propane was used to determine the angular correction factor, $F(\theta)$, from the following relationship:

$$F(\theta) = \frac{I_{\text{Prop},s}(90°)[1 + \cos^2\theta]}{I_{\text{Prop},s}(\theta)}. \tag{8}$$

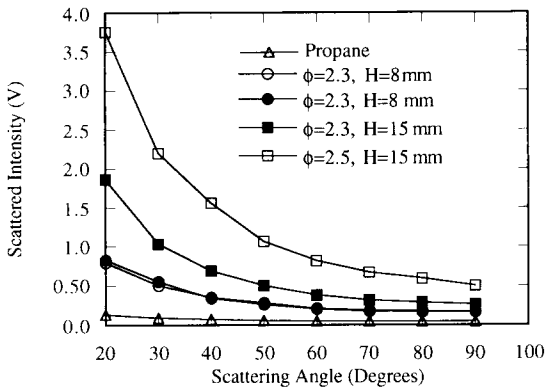

Fig. 7. Total scattered intensity as a function of scattering angle for an acetylene/air flame at various ϕ and H. Comparison with the data for propane is also provided.

The $F(\theta)$ term takes into account variation in the scattering volume as a function of scattering angle. The angular scattered intensities for the soot experiments were multiplied by the corresponding $F(\theta)$ terms and the differential scattering coefficients for soot were calculated using the following relationship:

$$\sigma_{\text{soot}}(\theta) = (\sigma_0 N_0)_{\text{Prop}} \frac{I_{\text{soot}}(\theta)}{I_{\text{Prop},s}(90°)} F(\theta) \left(\frac{I_{0\lambda}}{I_\lambda} \right), \tag{9}$$

where $I_{\text{soot}}(\theta)$ is the scattered intensity for soot, $(I_{0\lambda}/I_\lambda)$ is the ratio of the incident to transmitted light through the flame and $(\sigma_0 N_0)_{\text{Prop}}$ is the scattering coefficient for propane. The single particle scattering cross-section for propane at 488 nm, σ_0, is $9.57 \cdot 10^{-27}$ cm^2 [18]. The concentration of propane at ambient conditions (T = 298 K and P = 1 atm), N_0, is $2.46 \cdot 10^{19}$ molecules/cm^3.

Radius of gyration measurements were also performed to determine the size of the aggregates. For these experiments, the polarization angle was set at 90°. Figure 8 displays the $I_{vv}(q^2)/I_{vv}(0)$ as a function of q^2 (where $q = 4\pi \sin(\theta/2)/\lambda$) for various equivalence ratios. Measurements were performed at a height of 15 mm above the burner surface for all equivalence ratios. The angular correction factor $F'(\theta)$ (shown below) is different from $F(\theta)$ used in the total scattering measurements, because the magnitude of the (vv) component of the scattered signal is independent of scattering angle for Rayleigh molecules. $F'(\theta)$ was

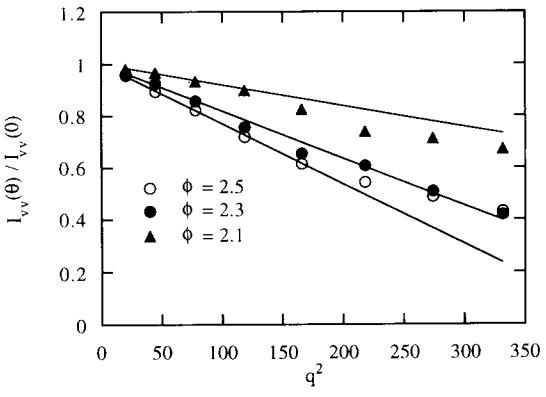

Fig. 8. $I_{vv}(\theta)/I_{vv}(0)$ as a function of q^2.

determined from the following equation:

$$F'(\theta) = \frac{I_{\text{Prop},s}(90°)}{I_{\text{Prop},s}(\theta)}. \quad (10)$$

The radius of gyration was calculated from the following equation with the assumption of small qR_g,

$$I(q) = I(0)\left[1 - \frac{1}{3}q^2\left(R_g^2\right)\right]. \quad (11)$$

The slopes of the least-squares fitted lines for small qR_g in Fig. 8 corresponds to $-R_g^2/3$. At equivalence ratios of 2.1, 2.3, and 2.5, the measured radii of gyration were 49 nm, 74 nm and 83 nm, respectively. These values are typically an order of magnitude smaller than the R_g measured for soot in the overfire region of turbulent diffusion flames burning acetylene and toluene [19]. For the overfire soot aggregates, the scattering to absorption ratios were typically of the order unity. However, due to the smaller soot aggregates measured in the present study, the scattering component of extinction is expected to be less important.

Figure 9 displays the differential scattering coefficients as a function of angle for the experiments presented in Fig. 7. The total scattering coefficient was calculated by integrating the differential scattering coefficients over the 4π solid angles. For the sootiest case ($\phi = 2.5$, $h = 15$ mm), the calculated scattering to absorption ratio $[\sigma_s/(K_\lambda - \sigma_s)]$ for the 488-nm wavelength was less than 8%.

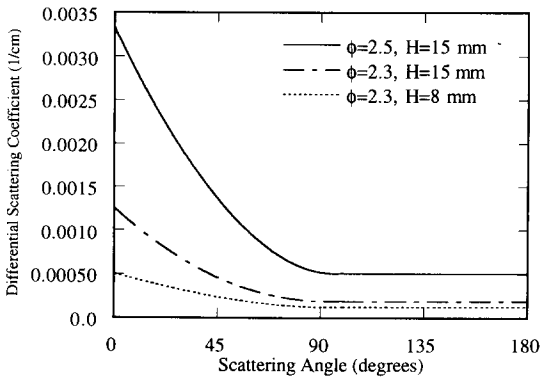

Fig. 9. Differential scattering coefficient as a function of scattering angle.

For a 633-nm source, the scattering to absorption ratio was estimated to be less than 4% using the following relationship (assuming a monodisperse particle size distribution [19]):

$$\rho_{sa} = \frac{2}{3}\left[\frac{\pi d_p}{\lambda}\right]^3 \frac{F(m)}{E(m)} n \times \left[1 + \frac{4}{3D_f}\left(\frac{2\pi}{\lambda}\right)^2 R_g^2\right]^{-\frac{D_f}{2}}, \quad (12)$$

$$F(m) = -\left|\frac{m^2 - 1}{m^2 + 2}\right|^2, \quad (13)$$

$$E(m) = -\text{Im}\left(\frac{m^2 - 1}{m^2 + 2}\right), \quad (14)$$

where the value of $m = 1.57 - 0.56i$, d_p is the particle diameter, λ is the source wavelength and n is the average number of particles per aggregate. This experiment demonstrates that the scattering/absorption ratio is too small to reconcile the large differences observed for f_{ve} and f_{va} measurements in the homogeneous premixed flame.

INFLUENCE OF THE SOOT INDEX OF REFRACTION

After eliminating the effects of soot scattering and light absorption by PAH molecules, the uncertainty in the refractive index (used to calculate the absorption constant) appears to be the most likely factor causing the discrepancy in the soot volume fractions in a homogeneous environment. Recent studies have questioned the practice of using a single set of refractive index (determined for soot generated from a particular fuel) for analyzing the radiative properties of soot generated from different fuels. In an early experiment, Dalzell and Sarofim [10] collected both acetylene soot [with a C/H ratio of 14.7] and propane soot [with a C/H ratio of 4.6] and measured only small differences between the optical properties of soot produced from the different fuels. In 1981, Lee and Tien [20] analyzed in situ transmittance measurements for several fuels and found variations in the indices of refraction. More recently, Habib and Vervisch [21]

analyzed soot produced from methane, propane and ethylene and found that in the visible and near-infrared wavelengths, the radiative properties of soot are dependent on the carbon to hydrogen ratio of the soot. In all of the above-mentioned work, the variables of the Drude-Lorentz dispersion model were varied to fit the transmittance or reflectance data. However, Felske and Ku [22] suggest that the use of the Drude-Lorentz dispersion relationship cannot be expected to produce accurate indices of refraction for a material such as soot (for which the properties are not well-characterized) when it can't predict the spectral features of a well-characterized material such as graphite.

Chang and Charalampopoulos [23] made in situ measurements of the refractive indices for soot produced in premixed propane flames using light scattering and the Kramers-Kronig relationship. They measured the index of refraction at various heights above the burner surface and found variations in both the real and imaginary components. They attributed this behavior to the changes in the chemical structure (i.e., C/H ratio) of soot. Sivathanu et al. [13] on the other hand measured the specific absorption constants for soot generated using premixed methane, propane and ethylene flames and found negligible differences. Thus, the conflicting conclusions regarding the impacts of physical and chemical effects on the optical properties of soot indicate the need for further work in this area [24].

The question arises as to which set of refractive index should be used to calculate the temperature and soot volume fractions. It is important to keep in mind that large variations in the measured T, f_{ve}, and f_{va} result when various sets of refractive index are used for the calculations. Figure 10 displays the absorption constant, K_λ, as a function of wavelength calculated from the refractive indices reported in the literature. The acetylene (D–S) corresponds to the experimentally measured values from Dalzell and Sarofim [10]. For the spectral range encompassing the visible to the near-infrared wavelengths, there are significant differences in the various sets of absorption constants. It is interesting to note that the three data sets of refractive index corresponding to

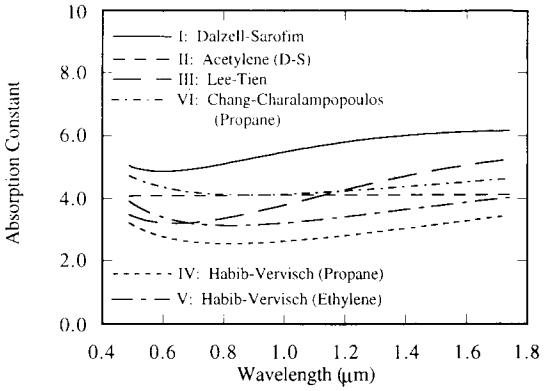

Fig. 10. Absorption constants calculated using various refractive indices reported in the literature.

soot from the same fuel (propane) produce large differences in K_λ. For example, at 633 nm, f_{va} calculated using Dalzell-Sarofim's data will be 50% smaller than the f_{va} determined using Habib-Vervisch's values. Thus, it appears that further in-situ testing over a wide range of parameters (including C/H ratio, d_p, R_g, etc.) may be necessary to determine the fuel effects on soot indices of refraction [24].

Using the six sets of absorption constants displayed in Fig. 10, the ratios of f_{va} and f_{ve} were calculated and plotted in Fig. 11. Since f_{ve} was measured using emission at 900 nm and 1000 nm, the best agreement with f_{va} should occur with absorption measurements performed at 940 nm. Such was not the case, because the f_{ve} measurements depend on the magnitude of the absorption constant and its variation as a function of wavelength, whereas f_{va} depends only on the magnitude of the absorption constant at the particular wave-

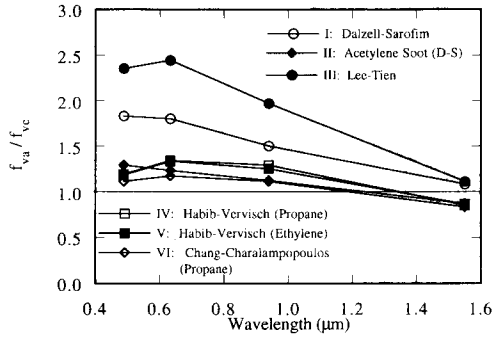

Fig. 11. f_{va}/f_{ve} ratio as a function of source wavelength using various sets of absorption coefficients.

length. Equations 3 and 4 show that the emission intensities are integrated from the lower to upper cutoff wavelengths of the interference filters (which ranged from 795 to 1085 nm). In this spectral range, the refractive index and therefore the calculated absorption constants vary significantly as a function of wavelength. For all cases however, the agreement between f_{va} and f_{ve} is improved for experiments using longer source wavelengths. In essence, the use of a longer wavelength source increases the range of validity (for sizes of soot particles/aggregates of interest in this study) of the Rayleigh-limit formulation used to calculate the absorption constants (see Eq. 2). The use of refractive index sets II, VI, V and VI resulted in the best agreement between the calculated f_{va} and f_{ve} over the wavelengths considered. However, the agreement between f_{va} and f_{ve} cannot serve as the sole basis for determining the "correct" set of absorption constants. The large uncertainties in the calculated absorption constant introduce significant uncertainties in both f_{va} and f_{ve}. For example, judicious choice of refractive index can produce a f_{va}/f_{ve} ratio of unity at all wavelengths, however the calculated f_{va} and f_{ve} may not represent the true measure of soot volume fraction. For this reason, it is desirable to measure the soot volume fraction independently of the optical properties of soot to determine a refractive index set that produces the best agreement.

SOOT SAMPLING EXPERIMENTS

In prior studies, isokinetic sampling experiments have been used primarily for analyzing particle/gas mixtures for conditions that are not far removed from the ambient. However, few studies have been performed in the high temperature environment of a premixed or diffusion flame. In this study, isokinetic soot sampling experiments were performed using a premixed acetylene/air flame for conditions identical to the experiments shown in Fig. 4 for direct comparison with the measured f_{va} and f_{ve}. Figure 12 displays the schematic diagram of the experimental arrangement. The probe

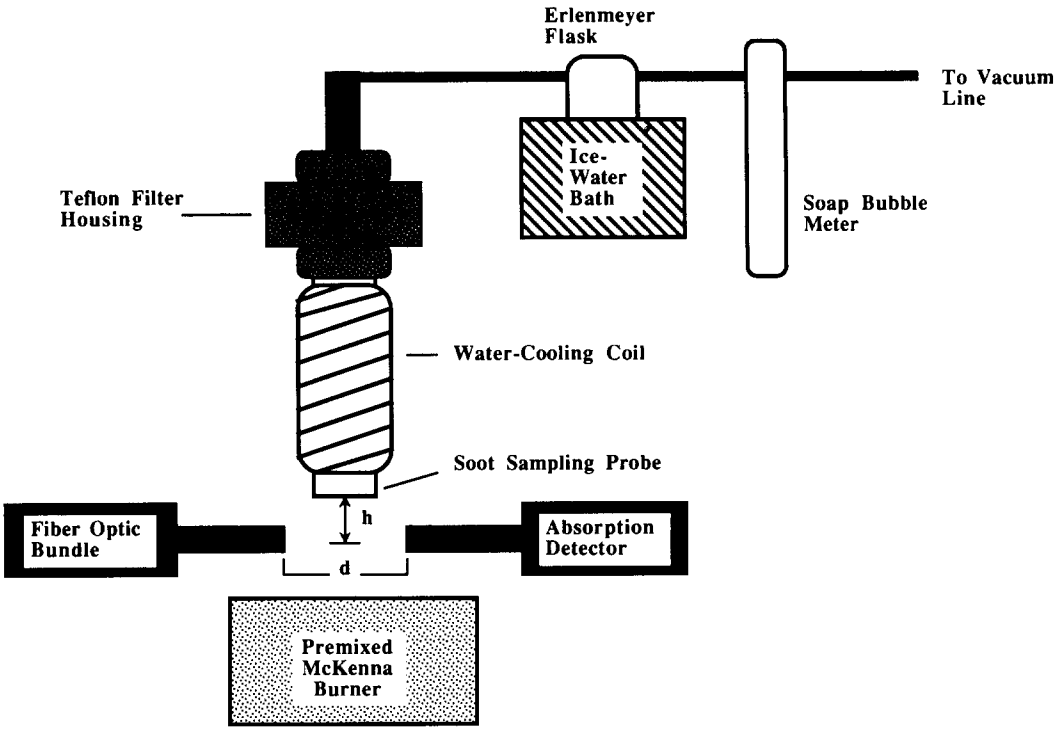

Fig. 12. Schematic of the isokinetic soot sampling experiment.

consists of a 9.6-mm stainless-steel pipe fitted with a Teflon filter assembly that has a collection efficiency greater than 99% for particles larger than 0.1 μm [25]. The probe was water-cooled with a 6.4-mm-diameter copper tube (starting at approximately 3 mm from the tip of the probe) to quench further reactions of soot as it traversed the length of the probe. Inevitably, there were substantial deposits of soot on the inner surface of the cold probe due to thermophoresis. The deposited soot was scrubbed from the probe and was included in the determination of the total soot mass collected within the 10 minute sampling period. Since the gas flow was measured at room temperature, the flow at the probe entrance was calculated from the ideal gas law by multiplying it by the ratio of the temperature at the inlet of the probe (obtained from emission measurements) to the ambient temperature. The flow was corrected for water condensation in the sampling probe (this increased the calculated flow by only a few percent). The soot volume fraction was calculated from the following formula:

$$f_v = \frac{\dfrac{m_s}{\rho_s}\dfrac{T_\infty}{T_{pe}}}{t\dfrac{dV}{dt}}, \tag{15}$$

where m_s is the dry mass of the collected soot (after being placed in an oven at 110°C for 15 hours), T_{pe} is the temperature at the probe entrance, T_∞ is the ambient temperature, t is the collection period, dV/dt is the volumetric flow rate and ρ_s is the density of soot (1.84 ± 0.1 g/cm^3). The density of soot was measured using Helium Pycnometry with soot collected on a stagnation plate placed 30 cm above the burner surface.

The effect of the sampling probe on the premixed flame structure was investigated by moving the sampling probe to various heights (Fig. 12) above the burner while simultaneously performing optical measurements using the three-line technique. With the distance between the optical probes, L, maintained at 30 mm, the sampling probe position above the optical line of sight, h, was varied. At a position of $h = 5$ mm (13 mm) above the burner surface, the measured temperature and soot volume fractions were essentially unchanged from the case in which the sampling probe was placed far downstream at $h = 50$ mm. Thus, at a height of 5 mm above the optical line of sight, the isokinetic sampling probe did not affect f_{ve} or the temperature measurements.

Table 1 compares the simultaneous measurements of the soot volume fraction determined from the isokinetic technique and f_{ve} (using 900 and 1000 nm) for an acetylene/air premixed flame ($\phi = 2.3$ at a height of 8 mm above the burner surface) using various sets of refractive index. The f_{ve} measurements using the various sets of index of refraction ranges from 0.40 to 0.97 ppm. The isokinetically measured soot volume fraction of 0.48 ppm is in good agreement with f_{ve} calculated using refractive indices sets I, II, and III, with a maximum discrepancy of only 25%. However, refractive index sets II and III produced f_{va}/f_{ve} ratios that were significantly greater than unity for wavelengths less than 1550 nm (Fig. 11). This experiment indicates that the f_{ve} calculated using the refractive index of acetylene soot [10] produced the best agreement with f_{va} and with the isokinetically measured value.

Although there are uncertainties with the isokinetic technique due to uncertainties associated with T_{pe}, ρ_s (see Eq. 15) and assumptions regarding the quenching of the soot reactions in the probe, it has provided an independent measure of the soot volume fraction that can be compared to the optically measured values.

TABLE 1

Comparisons of f_{ve} Calculated Using the Various Sets of Refractive Index with the Isokinetically Measured Values. f_{ve} Was Measured for $\phi = 2.3$ Acetylene/Air Flame at a Height of 8 mm Above Burner Surface

		f_{ve} (ppm)
I	Dalzell-Sarofim (Propane)	0.40
II	Dalzell-Sarofim (Acetylene)	0.60
III	Lee-Tien (PMMA)	0.45
IV	Habib-Vervisch (Propane)	0.97
V	Habib-Vervisch (Ethylene)	0.80
VI	Charamopopoulos-Chaing (Propane)	0.70
		f_v (ppm)
VII	Isokinetic Sampling Experiment	0.48

CONCLUSIONS

Temperature and soot volume fraction measurements in a homogeneous premixed flame environment resulted in a significant discrepancy between f_{va} and f_{ve}. Soot scattering experiments and experiments assessing the effect of light absorption by "large" molecules have confirmed that the common practice of using the Rayleigh-limit absorption constants of soot for optical measurements is valid for the conditions of the present study. However, the agreement between f_{va} and f_{ve} is dependent on the choice of refractive indices used to calculate the absorption constants. For all sets of absorption constants used in this study, the agreement in the soot volume fractions improved as the extinction source wavelength increased from 488 to 1550 nm. This is due to the reduced uncertainties in the literature values of the refractive indices and the validity of the Rayleigh-limit formulation to calculate the absorption constants.

The soot volume fraction measurements using isokinetic sampling techniques were used for comparisons with the optically determined values (using different sets of refractive index reported in the literature). Of the six sets of refractive index considered in this study, the refractive index for acetylene soot reported by Dalzell and Sarofim [11] produced the best simultaneous agreement of f_{ve} with the isokinetically measured values and with f_{va} at the four light extinction wavelengths that were considered.

The authors gratefully acknowledge the helpful discussion and advice provided by Drs. K. C. Smyth, W. L. Grosshandler, C. Shaddix and J. Harrington of NIST, Dr. G. H. Markstein of FMRC, Professor J. P. Gore of Purdue University, and Professor I. K. Puri of the University of Illinois at Chicago.

REFERENCES

1. Burgess, D. and Hertzberg, M., in *Heat Transfer in Flames* (N. H. Afgan and J. M. Beer, Ed.), Hemisphere Press, New York, 1974, p. 413.
2. Orloff, L., *Eighteenth Symposium (International) On Combustion*, The Combustion Institute, Pittsburgh, 1981, p. 49.
3. Fischer, S. J., Hardouin-Duparc, B. and Grosshandler, W. L., *Combust. Flame* 70:291– (1987).
4. Markstein, G. H., *Eleventh Symposium (International) On Combustion*, The Combustion Institute, Pittsburgh, 1981, p. 1055.
5. Klassen, M., Ph.D. dissertation, University of Maryland, Department of Mechanical Engineering, 1992.
6. Choi, M. Y., Hamins, A., Rushmeier, H., and Kashiwagi, T., *Submitted to the Twenty-Fifth Symposium (International) on Combustion*, in press.
7. Klassen, M., Sivathanu, Y. R., and Gore, J. P., *Combust. Flame* 90:34 (1992).
8. Cashdollar, K. L., *Appl. Opt.*, 18:2595 (1979).
9. Sivathanu, Y. R., Gore, J. P. and Dolinar, J., *Combust. Sci. Technol.* 76:45 (1991).
10. Dalzell, W. H. and Sarofim, A. L., *J. Heat Transf.* 91:100 (1969).
11. Harris, S. J. and A. M. Weiner, *Combust. Sci. Technol.* 31:156 (1983).
12. D'Alessio, A., Di Lorenzo, A., Sarofim, A. F., Beretta, F., Masi, S. and Venitozzi, C., *Fifteenth Symposium (International) on Combustion*, The Combustion Institute, 1974, p. 1427.
13. Sivathanu, Y. R., Gore, J. P., Janssen, J. M. and Senser, D. W., *ASME J. Heat Transf.* (in press).
14. Clar, E., *Polycyclic Hydrocarbons*, Academic, New York, 1964.
15. Weiner, A. M., and Harris, S. J., *Combust. Flame* 77:261 (1989).
16. D'Alessio, A., in *Particulate Carbon: Formation During Combustion* (D. C. Siegla and G. W. Smith, Ed.), 1981, p. 207.
17. Köylü, U. O., and Faeth, G. M., *Combust. Flame*, 89:140 (1992).
18. Landolt-Börenstein, *Optische Konstanten*, Springer, 1962, II. Band, i. Teil.
19. Dobbins, R. A., Mulholland, G. W. and Bryner, N. P., *Atmos. Environ.* (in press).
20. Lee, S. C., and Tien, C. L., *Eighteenth Symposium (International) On Combustion*, The Combustion Institute, Pittsburgh, 1981, p. 1159.
21. Habib, Z. G., and Vervisch, P., *Combust. Sci. Technol.* 59:261 (1988).
22. Felske, J. D., and Ku, J. C., *Combust. Flame* 91:1 (1992).
23. Chang, H., and Charalampopoulos, T. T., *Proc. R. Soc. Lond. A* 430:577 (1990).
24. Choi, M. Y., Mulholland, G. W., Hamins, A. and Kashiwagi, T., submitted to *Combust. Flame*.
25. Liu, B. Y. H., Pui, D. Y. H. and Bubow, K. L., *Aerosols in the Mining and Industrial Work Environments* (V. A. Marple and B. Y. H. Liu, Eds.), Ann Arbor Science, Ann Arbor, MI, 1983, Vol. 3, p. 989.

Received 18 August 1993; revised 20 April 1994

APPENDIX

Two approximations were made in estimating the total scattering intensity: First the differential scattering intensity for all $\theta > 90°$ is equal to the value at 90°, and secondly the scattering intensity for $\theta < 20°$ is obtained from an extrapolation of a linear fit of the data from 20° to 40°. The effect of these approximations on the total scattering is estimated using the following expression for the differential scattering by smoke agglomerates for unpolarized light [18]:

$$\sigma_{ag}(\theta) = \frac{AN^2(1 + \cos^2\theta)}{\left[1 + \frac{2}{3D_f}\left[R_g(4\pi/\lambda)\sin(\theta/2)\right]^2\right]^{D_f/2}}, \tag{16}$$

where

$$A = \frac{1}{2}k^4|\alpha|^2. \tag{17}$$

The quantity k is the wavenumber $2\pi/\lambda$, α is the polarizability, N, the number of primary spheres in the agglomerate, and D_f, the fractal dimension. The value of R_g was chosen so that the ratio of the scattering intensity at 20° and 90° is equal to the measured value and D_f is taken to be 1.8. The $\phi = 2.5$, $H = 15$ mm and the $\phi = 2.3$, $H = 8$ conditions correspond to $R_g = 145$ and 85 nm, respectively. For both conditions, the error in the total scattering coefficient associated with the linear extrapolation is less than 1%. Assuming a constant differential scattering intensity for $\theta > 90°$ results in about a 3% error of the total scattering coefficient for $R_g = 85$ nm and an error of less than 0.5% for $R_g = 145$ nm.